Metals Materials And Processes, 2000, Vol. 12, No. 2 & 3, pp. 281 - 292.

LATTICE STRAINS UNDER MEGABAR PRESSURES

A.K. Singh* and C. Balasingh
**CSIR Emeritus Scientist,*
Materials Science Division, National Aerospace Laboratories, Bangalore 560 017, India.

(Received 10 January 2000)

Abstract : The diamond anvil cell (DAC) can be used to compress samples to a few megabars, and the use of synchrotron radiation as a source of intense X-ray beam allows diffraction patterns to be recorded from the samples at such high pressures. Such experiments give information on the phase transitions and the lattice strains under pressure. Under truly hydrostatic pressure, the lattice strains conform to the symmetry of the unit cell. The pressure in the megabar region tend to deviate appreciably from the hydrostatic condition. The modeling of the non-hydrostatic stress in a DAC and its effect on the lattice strains are subjects of intense research activity. The analysis using appropriate theory of the lattice strain measured on a polycrystalline sample under non-hydrostatic condition can be used to estimate the shear strength and single crystal elastic moduli of the sample material as function of pressure. The pressure-volume relation of the sample material corresponding to hydrostatic compression naturally emerges from the analysis. This article reviews the experimental techniques and the present theoretical understanding of the non-hydrostatic effects.

Keywords : lattice strain, megabar pressures, diamond anvil cell, synchrotron radiation

1. INTRODUCTION

Pressure as a thermodynamic variable has attracted attention of the scientists in various disciplines. The goephysicists, who have contributed greatly to the development of the experimental techniques and theoretical aspects of large compression of solids, are interested in the experiments under the conditions that simulate the earth's interior. The experimental observation of phase transition under pressure and measurement of pressure-volume relation are of interest to the solid state physicists and material scientists, as these measurements provide a check on the *ab intio* theoretical calculations of the phase stability of solids. The scientists working in other areas have similar motivations to pursue studies at high pressure. The single most commonly used instrument in high pressure studies is diamond anvil cell (DAC). Excellent review[1] of the experimental techniques for different types of high pressure measurements using DAC can be found in literature. The pressure can be rendered truly hydrostatic by using metal gasket and fluid pressure transmitting medium. At very high loads, the pressure on the sample tends to become non-hydrostatic either when the pressure transmitting medium freezes, or the sample comes in contact with the anvils because of excessive thinning of the gasket. The X-ray diffraction from the compressed sample gives the *d*-spacings of the different sets of planes *(hkl)*. With reference to the *d*-spacings at the ambient pressure, the lattice strains can be calculated. These lattice strains conform to the symmetry of the unit cell if measured under truly hydrostatic pressure. For example, for a complete description of the lattice strains one linear compressibility is adequate for the cubic system whereas the hexagonal, trigonal, and tetragonal systems require two linear compressibilities, one along the *c*-axis and second along the *a*-axis. Once the pressure becomes non-hydrostatic, this *(hkl)*-dependence of the lattice strains becomes complex. In this article, we discuss the modeling of non-hydrostatic pressure and the theoretical development to describe its effect on the lattice strains measured by *in situ* X-ray diffraction. It is shown that the analysis of the lattice strains measured under non-hydrostatic compression gives the shear strength and single crystal elastic moduli as

function of pressure. The pressure-volume relation corresponding to the hydrostatic pressure can be also derived from this analysis.

2. STRESS STATE

The sample is pressurized by loading it between two flat and parallel faces of diamonds (Fig.1). As the stress on the sample exceeds the yield stress in compression, the sample begins to flow . This flow is opposed by the frictional force between sample and the anvil faces. The equilibrium thickness of the sample is decided by the coefficient of friction between the anvil face and the sample or the shear strength of the sample material depending on which of these two factors checks the flow of the sample[2-4]. The radial stress distribution is symmetric about the symmetry axis of DAC, and peaks at the center of the anvil[5,6]. The stress in the sample at the center of the anvil face is given by[7-12],

$$\sigma_{ij} = \begin{vmatrix} \sigma_{11} & 0 & 0 \\ 0 & \sigma_{11} & 0 \\ 0 & 0 & \sigma_{33} \end{vmatrix} = \begin{vmatrix} \sigma_P & 0 & 0 \\ 0 & \sigma_P & 0 \\ 0 & 0 & \sigma_P \end{vmatrix} + \begin{vmatrix} -t/3 & 0 & 0 \\ 0 & -t/3 & 0 \\ 0 & 0 & 2t/3 \end{vmatrix} = \sigma_P + D_{ij} \quad (1)$$

σ_{11} and σ_{33} are radial and axial stress components, respectively. σ_P is the mean normal stress and represents the equivalent hydrostatic pressure. The uniaxial stress component $t = (\sigma_{33} - \sigma_{11})$, and D_{ij} denotes the deviatoric stress component. Further, the maximum value of *t* is related to the yield strength of the specimen material[7,9],

$$t = (\sigma_{33} - \sigma_{11}) = 2\tau_y = \sigma_y \quad (2)$$

The symbols τ_y and σ_y denote shear strength and yield strength of the specimen material, respectively. The hydrostatic component, σ_P , can be expressed as,

$$\sigma_P = (\sigma_{11} + \sigma_{11} + \sigma_{33}) / 3 = (\sigma_{11} + t / 3) \quad (3)$$

The stress, σ_{ij}, as given by Eq. (1) is at point where the symmetry axis intersects the sample. This point coincides with the geometric center of the anvil-face. The off-diagonal terms are zero because of the axial symmetry about this point. Eq. (1) assumes that the anvil faces are flat and parallel, and do not deform under pressure. In practice, these conditions may not be fully satisfied. A detailed discussion of the effects of departure from the conditions on modeling is beyond the scope of this article. A brief discussion will be given later.

3. LATTICE-STRAIN EQUATIONS

It is to be noted that the sample used in these experiments are polycrystalline. The crystallites constituting the sample are single crystals and, in general, exhibit elastic anisotropy. The sample containing randomly oriented crystallites gives rise to Debye-Scherrer diffraction rings. The intensity at any point on a ring arises not from the crystallites of all possible orientations but only from those with definite orientation. As this point is central to the derivation of strain equations, we discuss it in some detail with reference to Fig. (1). Consider the incident beam, I_1. The diffraction ring recorded on a flat plate is a circle. This geometry is termed *parallel-geometry* and is most commonly used

for recording diffraction patterns using DAC. The orientation (with respect to the incident beam) of one of the crystallites that gives rise to the intensity at a point, A, is shown in Fig. (1b). The crystallites with orientations obtained by rotation about the plane normal, N, also contribute to the intensity at A. The plane normals of all such crystallites point in the direction, N. Crystallites with no other orientation contribute to the intensity at A. The angle, ψ , between N and the load direction, L, is an important parameter. It is seen that $\psi = (\pi / 2 - \theta)$and the value remains unchanged for all the points on the diffraction ring. Consider the incident beam, I_2, and assume that the sample occupies only a small region at the center of the anvil. It is possible to achieve this by placing the sample in a small hole at the center of a beryllium gasket. (Beryllium is nearly transparent to X-rays). The diffraction pattern recorded on a flat plate placed normal to I_2 are again concentric rings. As one moves from point, B, to point, C, along the diffraction ring, ψ smoothly changes from $\pi/2$ to θ . As seen later in this section, the lattice strain is a function of ψ. The strains in the crystallites that contribute to the intensity at different points on the ring are different. The diffraction rings under non-hydrostatic compression are, therefore, not circular when the incident beam (I_2) is perpendicular to the load axis. It may be noted that diffraction rings are perfectly circular for the incident beam (I_1). The diffraction geometry using the incident beam I_2 is termed *perpendicular geometry* and not commonly used with DAC.

As the load is increased, the hydrostatic component,σ_P, increases and constitutes the major stress component. At high pressures this component is large and so are the resulting strains. Such strains are interpreted best using a standard equation of state[13]. In magnitude, the deviatoric stress component, D_{ij}, is much smaller than the hydrostatic component. The *d*-spacing of a reflection *(hkl)* measured in presence of D_{ij} is given by the general relation[7,9-12],

$$d_m (hkl) = d_P (hkl)[1 + (1 - 3\cos^2\psi) Q (hkl)] \quad (4)$$

where $d_P(hkl)$ denotes the *d*-spacing in presence of the hydrostatic component alone. This quantity is not known, but required for determining the correct pressure-volume relation. Further,

$$Q(hkl) = \left(\frac{t}{3}\right)\left\{\alpha\left[2G_R^X(hkl)\right]^{-1} + (1-\alpha)(2G_V)^{-1}\right\} \quad (5)$$

$G_R^X(hkl)$, termed X-ray shear modulus, is the aggregate shear modulus calculated under the Reuss (iso-stress) condition. In calculating this quantity, the averaging is done only over the group of crystallites that contribute to the intensity at the point of observation. G_V is the aggregate shear modulus calculated under the Voigt (iso-strain) condition. The negative sign of *t* is included in Eq. (5), so that *t* is a positive quantity. The factor α decides, in an actual case, the relative weights of the strains calculated under Reuss and Voigt conditions. The value of α can lie between 0 and 1, but a realistic limit under the high-pressure condition α is between 0.5 and 1.

The expression for G_V in terms of S_{ij} can be found elsewhere[14]. The formalism for elasticity tensor followed in this article is given by Nye[15]. The expressions for $G_R^X(hkl)$ in terms of S_{ij} for all the seven crystal systems have been derived earlier[11,12,16]. To illustrate the power of this analysis, we consider here only cubic and hexagonal systems. For the cubic system,

$$\left[2G_R^X(hkl)\right]^{-1} = \left[S_{11} - S_{12} - 3S\Gamma(hkl)\right] \tag{6}$$

where $S = \left(S_{11} - S_{12} - \frac{1}{2}S_{44}\right)$

$$\Gamma(hkl) = \left(h^2k^2 + k^2l^2 + l^2h^2\right) / \left(h^2 + k^2 + l^2\right)^2 \tag{7}$$

For the hexagonal system,

$$\left[2G_R(hkl)\right]^{-1} = \frac{1}{2}\left[(2S_{11} - S_{12} - S_{13}) + I_3^2(-5S_{11} + S_{12} + 5S_{13} - S_{33} + 3S_{44}) + I_3^4(3S_{11} - 6S_{13} + 3S_{33} - 3S_{44})\right] \tag{8}$$

$$I_3^2 = 3a^2l^2 / \left[4c^2\left(h^2 + hk + k^2\right) + 3a^2l^2\right] \tag{9}$$

a and c are the lattice parameters of the hexagonal cell at a pressure σ_P. The S_{ij}-terms appearing in these equations also are at a pressure σ_P.

3. EXPERIMENTAL TECHNIQUES

Eq. (4) is valid for all the seven crystal systems and suggests that $d_P(hkl)$ and $Q(hkl)$ can be obtained from the dm(hkl) versus $(1\text{-}3\cos^2\psi)$ plot. In the commonly used mode for recording diffraction patterns with a DAC, one uses the geometry (parallel geometry) with incident beam I_1 as shown in Fig. (1). The wavelength of the X-rays used for these measurements has to be necessarily short (in the range of 0.05 to 0.07 nm) to reduce the absorption in the diamond anvils. Consequently, the reflections occur at small θ -values in angle-dispersive mode of data recording. Since $\psi = (\pi / 2 - \theta)$ for this geometry, ψ -values do not change appreciably over the entire range of recorded reflections. Even though the small changes in ψ were used to get meaningful values of S_{11} / S and $(S_{11} - S_{12})$ / S for sodium chloride[17], a data over wider range of ψ will give better reliability . Recording of data over wide range of ψ obviously required modification of the diffraction geometry. With the perpendicular geometry (Fig. 1), recording of the data with ψ in the range θ to $\pi / 2$ is possible. In fact, this geometry was used to study the non-hydrostatic compression effect on the lattice strains[18]. In this study, the incident beam traversed through the entire region of the stress differential in the sample that ranged from the highest pressure at the center of the anvil to nearly one atmosphere at the edges. This made the interpretation of the data rather difficult. To overcome this problem, the use of beryllium or boron gasket to confine the sample over a small region at the center of the anvil was suggested[19]. A similar concept using tungsten carbide anvils and boron gasket was successfully tried[20]. The use of tungsten carbide anvils, however, limited the highest attainable pressure to about 20 GPa. The most versatile geometry that permitted data recording over the entire range of ψ, from 0 to $\pi / 2$, used the energy-dispersive method of data recording[21] shown in Fig. (2). The sample is contained in a small hole (30 μm in diameter) at the center of a beryllium gasket. The use of any pressure transmitting medium is deliberately avoided to enhance the non-hydrostatic effects. The gasket with the sample at the center is placed on the diamond anvil face (400 μm). The beryllium gasket confines the sample over a small region around the center of the anvil face, and thereby, minimizes the radial pressure gradient in the sample. A fine beam (5-10 μm in diameter) from a synchrotron source enters the gasket at small angle θ (5-10°) to the anvil face and illuminates the

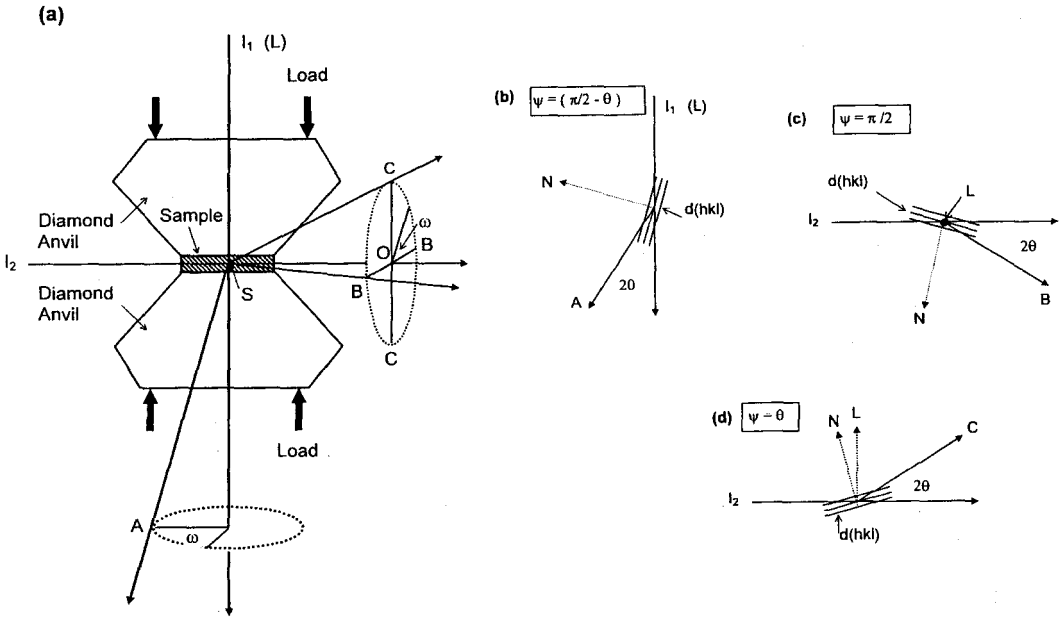

Fig. (1) (a) Different possible diffraction geometry with a DAC. (b) - (d) Orientation of the crystallites with respect to the load axis, L. The angle between the diffracting-plane normal, N, and L is denoted by ψ. The ψ-value depends on the point of observation on the diffraction ring.

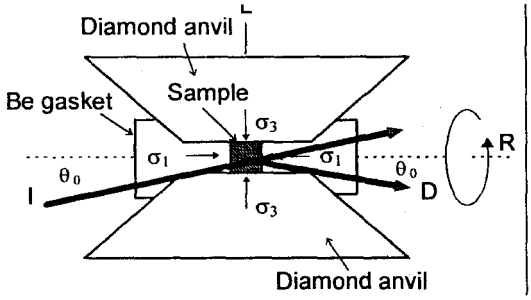

Fig. (2) The diffraction geometry with a DAC that permits any setting of the angle,ψ.

sample. The diffraction patterns are recorded using an energy-dispersive detector with its line-of-sight making angle θ with the anvil face. The ψ angle is chosen by rotating the entire DAC assembly about the axis R. At any setting, all the reflections are recorded with the same ψ. It is possible to secure a precise alignment such that the volume defined by the intersection of the incident beam and the line-of-sight of the detector is confined to the sample volume, and does not overlap with any part of the gasket. In such a case, the diffraction pattern from the gasket can be discriminated. This is possible only in the energy-dispersive mode[22].

4. DATA AND INTERPRETATION

The geometry shown in Fig. (2) was first used[23] to measure *d*-spacings in FeO at different ψ values at pressures up to 25 GPa. Below 16 GPa, FeO is cubic and transforms to a rhombohedral structure. The observed dependence of d_m(hkl) on ψ in a typical case is shown in Fig. (3a). In accordance with Eq. (4), the d_m(hkl) versus (1 - $3\cos^2\psi$) plot is found to be a straight line. The large volume of data on a number of materials belonging to cubic, hexagonal, and rhombohedral systems analyzed so far are found to fit Eq.(4)

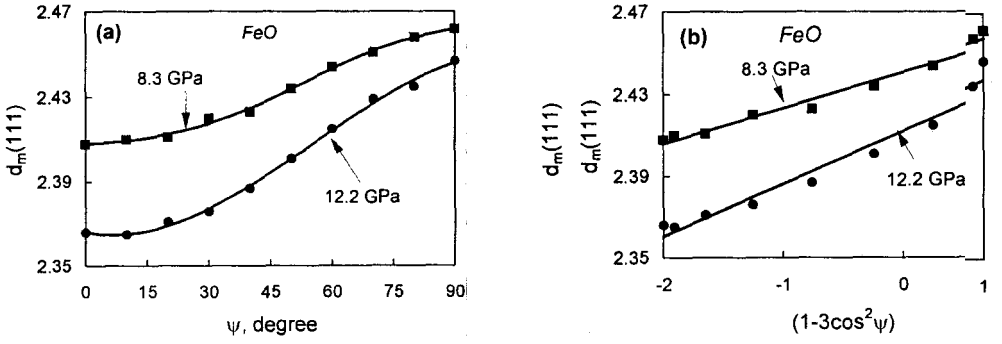

Fig. (3) (a) versus data for FeO. (b) Same data set shown as versus plot.

Table I. Analysis of lattice parameters obtained from d_P(hkl). The numbers in the parentheses indicate the standard errors (last decimal place)

P (GPa)	FeO (fcc) 8.3	FeO (rhomb.) 19	α-Fe (bcc) 4.6	ε-Fe (hcp) 52
a_P (Å)	4.230(2)	2.887 (3)	2.8417 (9)	2.3736 (7)
a_ψ	4.252 (11)	2.891 (10)	2.8482 (15)	2.3810 (60)
c_P	-	7.344 (10)	-	3.7896 (3)
c_ψ	-	7.428 (60)	-	3.7950 (20)
$V_P(Å)^3$	75.67 (6)	53.01 (13)	22.948 (12)	36.98 (2)
V_ψ	76.85 (34)	53.77 (57)	23.105 (20)	37.25 (18)

very well. The slope and the intercept of d_m(hkl) versus $(1 - 3\cos^2\psi)$ plot can be used to obtain the d_P(hkl) and Q(hkl) for each reflection.

4.1 *d*- spacings under σ_P

The lattice parameters, denoted by a_P and c_P, calculated from the d_P(hkl)-values obtained from the d_m(hkl) versus $(1 - 3\cos^2\psi)$ plots in a few cases are listed in Table I. For comparison, the lattice parameters, denoted by a_ψ and c_ψ, calculated from the d_m(hkl)-values at $\psi = 85^o$ are also listed. The parameters, a_ψ and c_ψ, approximately correspond to the values obtained, ignoring the non-hydrostatic effects, from the measurements in the parallel geometry. It is clearly seen that the standard deviations in a_ψ and c_ψ are much larger than the corresponding numbers for a_P and c_P . This indicates that the distortion of the unit cell caused by D_{ij} is appreciable and d_P(hkl) truly represents the *d*-spacings under hydrostatic compression. The equation of state of solids (pressure-volume relation) derived from d_P(hkl) will be close to that obtained under hydrostatic compression. It is seen from Eq. (4) that the measured *d*-spacing at $\psi_c = \cos^{-1}(1/\sqrt{3})$ corresponds to d_P(hkl). Thus, measurement at a single setting at ψ_c can give d_P(hkl) . The information on Q(hkl), however, is lost. The measurements at a number of ψ -values are desirable, as the reliability in the estimation of d_P(hkl) can be improved. Further, it is seen that the unit cell volumes are overestimated (the volume strains underestimated) if the non-hydrostatic compression effects are ignored. This fact was realized quite early in the development of this field[24,25] and has been re-emphasized recently while discussing the non-hydrostatic compression of molybdenum[26].

4.2 Estimation of *t*

As discussed earlier, *t* places a lower limit on the shear strength of the sample material. The present analysis offers an elegant way to determine this limit as a function of

pressure. Two different approaches have been used in the literature to estimate *t*. A group of investigators[27-30] used isotropic elasticity theory while others used lattice strain theory to analyze the diffraction data[20, 31-35]. The use of the lattice strain equations requires the knowledge of the single crystal elastic moduli which are obtained by the extrapolation of the moduli at one atmosphere using the pressure derivatives. The following relation for the cubic system can be derived from Eqs. (4) and (5),

$$t = (6G)\langle Q(hkl)\rangle f(x) \tag{10}$$

$$f(x) = A / B$$

$$A = \{[(2x + 3) / 10] + 5x / 2(3x + 2)\}$$

$$B = \{\alpha[x - 3(x - 1)\langle\Gamma(hkl)\rangle] + 5x(1 - \alpha) / (3x + 2)\}$$

where the angle brackets denote the average over all the observed reflections. *G* is the aggregate shear modulus at a pressure, σ_P. The term, $x = 2(S_{11} - S_{12}) / S_{44}$, represents the elastic anisotropy. For the case of elastic isotropy (x=1), $f(x)=1$. Even for moderately large anisotropy, $f(x) \cong 1$. In most cases, Eq. (10) with $f(x) = 1$ can be used to estimate *t* using the Q(hkl) values for cubic as well as other systems. The aggregate shear modulus at high pressure can be obtained by the extrapolation of the one atmosphere value.

4.3 Analysis of Q(hkl)

An attempt was made earlier[17] to derive partial information on S_{ij} by analyzing the DAC data. The estimation of S_{ij} from the analysis of Q(hkl) was suggested for the first time by Singh et.al[36] and the details were subsequently reported in a number of articles[12,26, 37,38].

4.3.1 Cubic system : It is seen from Eqs. (5)-(7) that a plot of Q(hkl) versus Γ(hkl) is a straight line. Such a plot is shown in Fig. (4). The slope, m_0, and intercept, m_1, of this line are given by,

$$m_0 = -(\alpha t / 3)\left[S_{11} - S_{12} - \tfrac{1}{2} S_{44}\right]$$

$$m_1 = (t / 3)\left[\alpha(S_{11} - S_{12}) + \tfrac{5}{2}(1-\alpha)\frac{(S_{11} - S_{12})S_{44}}{3(S_{11} - S_{12}) + S_{44}}\right] \tag{11}$$

and,

$$m_1 / m_0 = -\left[x / (x-1) + 5(\alpha^{-1} - 1)x / (x-1)(3x\right. \tag{12}$$

Eq. (12) suggests that the elastic anisotropy can be determined from Q(hkl) versus Γ(hkl) plots. This will require the knowledge of α, which is not known *a priori*. As discussed earlier, realistic limits of α are *0.5* and *1*. For a given ratio (m_1 / m_0), the value of x obtained from Eq. (12) is sensitive to the choice of α. For example, for (m_1 / m_0) = 2, x decreases by a factor 3 when α is changed from *1* to *0.5*. The lowest estimate of the elastic anisotropy is obtained with α = 1. For a number of metals, a good agreement is found between the elastic anisotropy obtained with α = 1 and that obtained from the extrapolated elastic moduli measured by ultrasonic technique. This seems to indirectly suggest that the iso-stress condition is valid for ductile materials. Is the limit of α =

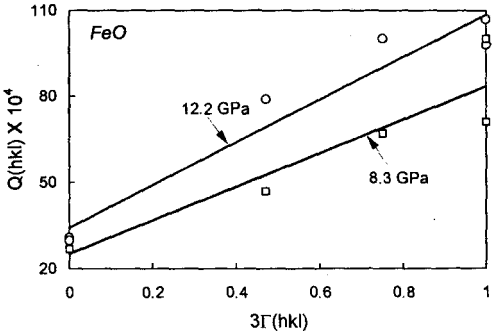

Fig. 4. Q(hkl) versus Γ(hkl) plot for FeO.

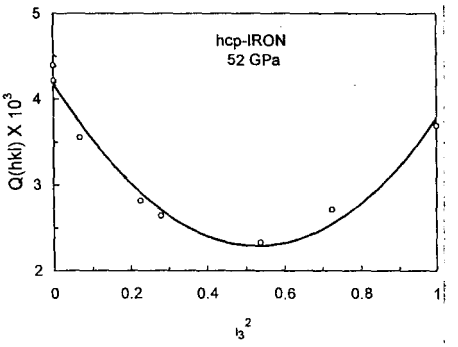

Fig. 5. Q(hkl) versus I^2_3 for ε-iron (hcp) at 52 GPa..

0.5 reached for the brittle materials? This conjecture can be verified when data on such materials becomes available.

It is possible to estimate S_{ij} using Eqs. (9) - (11) and the linear compressibility which for the cubic system equals $(S_{11} + 2S_{12})$. The S_{ij} values of molybdenum, gold, iron, and FeO have been determined[16,26,38] as a function of pressure. These values are in good agreement with the corresponding values obtained from the extrapolation of the elasticity data determined by ultrasonic technique.

4.3.2 Hexagonal system : It is seen from Eqs. (4), (5), and (8) that the Q(hkl) versus I_3^2 plot for the hexagonal system is a parabola of the type,

$$Q(hkl) = m_0 + m_1 I_3^2 + m_2 I_3^4 \tag{13}$$

where,

$$m_0 = (\alpha t / 6)\left[2S_{11} - S_{12} - S_{13} + (\alpha^{-1} - 1)(2G_V)^{-1}\right] \tag{14a}$$

$$m_1 = (\alpha t / 6)\left[-5S_{11} + S_{12} + 5S_{13} - S_{33} + 3S_{44}\right] \tag{14b}$$

$$m_2 = (\alpha t / 6)\left[3S_{11} - 6S_{13} + 3S_{33} - 3S_{44}\right] \tag{14c}$$

In addition to the three relations given by Eqs. (14 a-c), two more relations are provided by the axial compressibilities,

$$\chi_a = \alpha\,(S_{11} + S_{12} + S_{13}) + (1 - \alpha)\,(3K_V)^{-1} \tag{15a}$$

$$\chi_c = \alpha\,(S_{33} + 2S_{13}) + (1 - \alpha)\,(3K_V)^{-1} \tag{15b}$$

As expected, the Q(hkl) versus I_3^2 plot for a hexagonal system shown in Fig. (5) is a parabola. The details of the calculations can be found elsewhere[12,36,38]. The C_{ij} values obtained by this method for cubic and hcp iron and cubic FeO are listed in Table II. It may be noted that there is a significant discrepancy between the elastic moduli of ε-iron obtained by this technique and those from *ab initio* calculations[12,33]. This aspect is discussed in a recent article[39]. A similar discrepancy is observed for rhenium[38]. A review of the work done prior to 1993 can be found elsewhere[37]. The equations for all the seven crystal systems have been derived, though the lower symmetry systems have not been analyzed using these equations.

5. SOME FURTHER COSIDERATIONS

The experimental conditions in an actual case may deviate significantly from those implicitly assumed in the development of the theory. It is important to examine the effect of the departure from assumed conditions on the lattice strain equations discussed here. Eq. (1) is derived assuming that the anvil faces are flat, parallel, and perfectly rigid. To start with, a very high degree of flatness and parallelism of the anvil faces can be achieved by using suitable techniques. However, both the flatness and parallelism of the anvil faces get affected under high pressure. The diamond anvils have high hardness but can undergo large deformations[34] mostly in the form of cupping. For symmetric cupping, the axial symmetry is retained, and Eq. (1) is still valid, though the magnitudes of the stress components get effected. The loss of parallelism of the anvil faces together with cupping introduces asymmetry in the stress state. The asymmetry is introduced even in a perfectly aligned set up if the incident X-ray beam does not fall at the geometric center of the sample. The lack of axial symmetry results in the appearance of the off-diagonal terms in Eq. (1). As discussed in detail elsewhere[40], the non-zero off-diagonal terms lead to a large non-linearity in the $d_m(hkl)$ versus $(1 - 3\cos^2\psi)$ plot. The sample is assumed to contain randomly distributed crystallites. The sample undergoes considerable plastic deformation on compression between the anvil faces and develops preferred orientation (texture). The presence of texture also leads to non-linearity in the $d_m(hkl)$ versus $(1 - 3\cos^2\psi)$ plot[40]. The equations have been derived assuming an equal t acting on the crystallites of different orientations with respect to the load direction. If we extend the analogy of the single-crystal deformation which is strongly orientation dependent, then this assumption appears difficult to justify. The deformation of the crystallites of a polycrystalline sample is extremely complex. Each crystallite is constrained by the neighboring crystallites. This necessitates that the deformation of each crystallite should conform to the deformation of its neighbors[40]. The linearity of the $d_m(hkl)$ versus $(1 - 3\cos^2\psi)$ plots is a good indication of reasonable alignment of the experimental set up.

These equations have been applied in different areas. The elastic moduli of ε-iron were determined to 220 GPa, and these data were used to interpret the anomaly in the seismic wave velocity in the earths inner core[41]. The hot-pressed C_{60} samples give unusual diffraction patterns in that the diffraction rings are elliptical when recorded on a flat image-plate with the incident beam normal to the load axis during hot pressing[42]. This effect arises due to large locked-in stresses in C_{60} during the hot pressing. The ellipticity of the diffraction rings can be analyzed using these equations to estimate the magnitudes of the locked-in stresses.

A comment on the isotopic elasticity theory (IET) developed by many investigators[18,28-30] and used to interpret the lattice strains is in order. The argument put forward in favor of the IET as applied to the X-ray diffraction from the stressed samples is that the sample containing randomly oriented crystallites is elastically isotropic. As discussed at length in earlier articles[10,11], this line of argument is misleading. The present equations reduce to those obtained by the IET, if the crystallites of the sample are isotropic. The differences between the two theories diverge as the elastic anisotropy of the crystallites increases. However, the IET provides adequate description so far as the determination of t is concerned.

The attractive feature of this analysis is its ability to give t and the single-crystal elastic moduli from the diffraction data on polycrystalline sample to a few hundred gigapascals.

No other technique exists at present which can match this pressure range. There are many other unique features of this analysis. The present technique does not require good quality single crystals as is the case with either the ultrasonic technique or the technique using Brillouin scattering[42,43]. The sample size used is extremely small ($\cong 10^{-15}$ μm). Further, this appears to be the only technique, apart from first principle theoretical calculations[44,45], that can be used to measure the elastic moduli of the pressure-induced metastable phases. The point to be kept in mind is that there are still some uncertainties in the estimation of the elastic moduli of the hexagonal system. The overall precision in the estimation of the moduli is rather poor. This disadvantage has to be weighed against the advantages of this technique listed above.

6. CONCLUSIONS

(1) The non-hydrostatic stress state of the sample in the megabar pressure range can not be avoided.

(2) Only the theory based on the anisotropic elasticity, as discussed here, explains all the features observed in the diffraction patterns from the samples compressed in a diamond anvil cell.

(3) The stress state at the center of the sample compressed in a diamond anvil cell is adequately described by Eq.(1), for the samples containing randomly oriented crystallites. Even in the presence of texture, it provides a reasonable description.

(4) The linearity of the $d_m(hkl)$ versus $(1-3\cos^2\psi)$ plots is general and indicates the correctness of the setup alignment. The slope and the intercept of the straight line drawn through the data give $d_P(hkl)$ and Q(hkl). The $d_P(hkl)$ represents the *d*-spacings under the hydrostatic component . This information can be used to obtain equation of state corresponding to hydrostatic compression from the data under non-hydrostatic compression. Q(hkl) contains information on the single-crystal elastic moduli and the uniaxial stress component *t*. The Q(hkl), when averaged over *(hkl)*-space, gives estimates of *t*. The single-crystal elastic moduli can be obtained if the data on the axial compressiblties is used. Both, *t* and the elastic moduli estimated from this analysis are at a pressure σ_P

(5) The formalism used in the development of the strain equations can also be used to discuss the effect of a tri-axial stress system on the *d*-spacings.

ACKNOWLEDGEMENTS

The development of the lattice-strain equations as applied to the present problem started more than 25 years ago. Rapid advancements made in the recent years are due to the fact that a number of researchers have picked up this area of activity. I (AKS) place on record extremely fruitful collaboration with H. K. Mao and R. J. Hemley (Carnegie Institution of Washington), and T. S. Duffy (Princeton). Also placed on record are the discussions with R. E. Cohen (Carnegie Institution of Washington) and D. J. Weidner (SUNY, Stony Brook).

REFERENCES

1. Jayaraman, A. , Rev. Sci. Instrum., 1986, **57**, 1013.
2. Schroeder, W, and Webster, D. A., J. Appl. Mech., 1949, 289.
3. N. H. Palokowski, and E. J.Ripling, Strength and Structure of Engineering Materials, Prentice Hall, N. J., 1966.

4. P. Van Houtte, in: Numerical Modeling of Material Deformation Processes, Eds., P. Hartley, I. Pillinger, and C. E. N. Sturgess, Springer, London, 1992.
5. Sung,C. M., Goetze, C., and Mao, H. K., Rev. Sci. Instrum., 1977, **48,** 1386.
6. Kimura, H., Ast, G., and Bassett, J. Appl. Phys., 1982, 53, 3523.
7. Singh, A. K., and Kennedy, G. C., J. Appl. Phys., 1974, **45**, 4686.
8. Ruoff, A. L., J. Appl. Phys., 1975, **46**, 1389.
9. Singh, A. K., J. Appl. Phys., 1993, **73**, 4278.
10. Singh, A. K., J. Appl. Phys., 1993,**74**, 5920.
11. Singh, A. K., and Balasingh. C., Bulletin Mater. Sci., 1996, **19**, 601.
12. Singh, A. K., Balasingh, C., Mao, H. K., Hemley, R. J., and Shu, J., J. Appl. Phys., 1998, **83**, 7567.
13. Holzapfel, W. B., Rep. Prog. Phys., 1996, **59**, 29.
14. Hearmon, F. R. S., Adv. Phys., 1956, **5**, 323.
15. J. F. Nye, Physical Properties of Crystals, Oxford University Press, London, 1960.
16. Uchida, T., Funamori, N., and Yagi, Y., J. Appl. Phys., 1996, **80**, 739.
17. Usha Devi, S., and Singh, A. K., Physica, 1986, **139-140 B**, 922.
18. Kinsland, G. L., and Bassett, W. A., Rev. Sci. Instrum., 1976, **47**, 130.
19. Singh, A. K., in High Pressure Science and Technology-1993, AIP Conf. Proc. No. 309, API, New York, 1994, p.1629.
20. Funamori, N., Yagi,T., and Uchida, T., J. Appl. Phys., 1994, **75**, 4327.
21. Mao, H. K., and Hemley, R. J., High Press. Res., 1996, **14**, 257.
22. Singh, A. K., and Usha Devi, S., Bulletin Mater. Sci., 1987, **9**, 225.
23. Mao, H. K., Shu, J., Fei, Y., Hu, J., and Hemley, R. J., Phys. Earth Planet. Inter., 1996, **96**, 135.
24. Sato, Y., Ida, Y., and Akimoto, S., High Temp.-High Press., 1973, **5**, 679.
25. Singh, A. K., High Temp.-High Press., 1978, **10**, 641.
26. Duffy, T. S. et al, J. Appl. Phys., 1999, **86**, 6729.
27. Meade, C., and Jeanloz, R., J. Geophys. Res., 1988, **93**, NO. B4, 3261.
28. Ruoff, A. L., Xia, H., Lu, H., and Vohra, Y. K., Rev. Sci. Instrum., 1990, **61**, 3830.
29. Jeanloz, R., Godwal, B. K., and Meade, C., Nature (London), 1991, **349**, 687.
30. Meng, Y., Wedner, D. J., and Fei, Y., Geophys. Res. Lett., 1993, **20**, 1147.
31. Singh, A. K., and Kennedy, G. C., J. Appl. Phys. 1976, **47**, 3337.
32. Singh, A. K., Philos. Mag. Lett., 1993, **67**, 379.
33. Duffy, T. S., Hemley, R. J., and Mao, H. K., Phys. Rev. Lett., 1995, **74**, 1371.
34. Hemley, R. J., et al, Science, 1996, **276**, 1242.
35. Wolanin, E., et al, Phys. Rev. B,1997, **56**, 1997, 5781.

36. Singh A. K., Mao, H. K., Shu, J., and Hemley, R. J., Phys. Rev. Lett., 1998, **80**, 2157.

37. Singh A. K., Balasingh, C., Mao, H. K., Shu, J., and Hemley, R. J., Rev. High Pressure Sci. Technol., 1998, **7**, 205.

38. Duffy, T. S., et al, Phys. Rev. B, 1999, **60**, 15063.

39. Singh, A. K., Balasingh, C., Mao, H. K., Hemley, R. J., and Duffy, T. S., in: Proc. of the Int. School on Powder Diffraction, Ed., S. P. Sengupta, Allied Publishers, New Delhi, 1998, pp 64-77.

40. Mao, H. K., et al, Nature, 1998, **396**, 741.

41. Marques, L., et al, Science ,1999, **283**, 1720.

42. Zha, C. S., Duffy, T. S., Mao, H. K., and Hemley, R. J., Phys. Rev. B, 1993, **48**, 9246.

43. Shimizu, H., Ohnishi, M., Sasaki, S., and Ishibashi, Y., Phys. Rev. Lett., 1995, **74**, 2820.

44. Stixrude, L., and Cohen, R. E., Science, 1995, **267**, 1972.

45. Soderlind, P., Moriarty, J. A., and Wills, J. M., Phys. Rev. B, 1996, **53**, 14.

46. Jackson, I., Kahanna, S. K., Revcolevsci, A., and Berthon, J., J. Geophys. Res. 1990, **95**, 21671.

47. Guinan, M. W., and Besher, D. N., J. Phys. Chem. Solids, 1968, **29**, 541.